Trapping and Beamloading in hybrid Plasma Wakefield Accelerator schemes

Alexander Knetsch

November 18, 2016

CONTENTS

1. THEORY

1.1 The history of wakefield acceleration

Tajima Dawson great Idee, MTV bubble regime, same time PWFA von Rosenzweig... first linear measurements for PWFA

1.2 Plasma physics

There are several definitions of a plasma, but one of the most appealing one that we will follow in this work can be found in the classic textbook by Francis F. Chen: "A plasma is a quasineutral gas of charged and neutral particles which exhibits collective behavior" [1]. Regarding the gas types we will conveniently assume them to be electrons, ions and neutral atoms and comment that other particles as well can fit the definition of a plasma, but such exotic compositions are beyond the scope of this work.

Debye Shielding

The concept of *quasi-neutrality* roots in the shielding behavior of the ions and electrons of charges inside the plasma. A positive net charge e.g. originating from a difference in ion density n_i and electron density n_e at a temperature T would attract electrons and lead to an electron distribution

$$f(u) \propto \exp(-\frac{1}{2}m_\mathrm{e}v^2 + q_\mathrm{e}/(k_\mathrm{B}T)). \tag{1.1}$$

With the Poisson Equation

$$\begin{aligned} \epsilon_0 \frac{d^2\Phi}{dx^2} &= -q_\mathrm{e}(n_\mathrm{e} - n_\mathrm{i}) && (1.2)\\ &= q_\mathrm{e}n_\mathrm{e}(\exp(q_\mathrm{e}\Phi/(k_\mathrm{B}T)) - 1) && (1.3)\\ &\approx q_\mathrm{e}n_\mathrm{e}(q_\mathrm{e}\Phi/(k_\mathrm{B}T) + ...) && (1.4) \end{aligned}$$

we can now derive the potential in the plasma

$$\Phi = \Phi_0 \exp(-|x|/\lambda_\mathrm{D}) \tag{1.5}$$

with the information about the range of the shielded Coulomb field embedded in the Debye Radius

$$\lambda_\mathrm{D} = \sqrt{\frac{\epsilon_0 k_\mathrm{B}T}{n_\mathrm{e}q_\mathrm{e}^2}}. \tag{1.6}$$

We can see that a plasma with an edge length $L >> \lambda_\mathrm{D}$ would have its Coulomb fields shielded and appear to an outside observer to be charge-neutral.

Plasma frequency

Electrons and ions in a plasma can be described as two fluids, each following the fluid dynamics and interacting via the Maxwell Equations and collisions.

If the electron fluid is displaced with respect to the ion fluid this leads to strong electric fields, acting upon both as a restoring force, but as $m_\mathrm{i} >> m_\mathrm{e}$, the electron response is much quicker which is why these kind of plasma oscillations are dominated by the electrons, while the ions can be considered inert.

Starting from equation (1.2) with the relation of the electric field and its potential being $\vec{E} = -\nabla\Phi$

$$\epsilon_0 \nabla \vec{E} = q_\mathrm{e}(n_\mathrm{i} - n_\mathrm{e}) \tag{1.7}$$

becomes for small perturbations $n' = n_\mathrm{e} + \delta n$

$$\epsilon_0 \nabla \vec{E} = q_\mathrm{e} \delta n). \tag{1.8}$$

The solution to this differential equation is a harmonic density oscillation

$$n(x,t) = \delta n \exp(i(kx - \omega_\mathrm{p} t)). \tag{1.9}$$

The characteristic frequency of this oscillation

$$\omega_\mathrm{p} = \sqrt{\frac{n_\mathrm{e} q_\mathrm{e}^2}{\epsilon_0 m_\mathrm{e}}} \tag{1.10}$$

is called the *Plasma frequency* and is one of the most important parameters in plasma physics. In the field of PWFA it is convenient to also consider the wavelength associated with the plasma oscillations, the *Plasma wavelength*

$$\lambda_\mathrm{p} = 2\pi \frac{\omega_\mathrm{p}}{c}. \tag{1.11}$$

Typical values for example for a plasma density $n_\mathrm{e} = 1 \times 10^{17}\mathrm{cm}^{-3}$ are

$$\begin{aligned} \omega_\mathrm{p} &\approx 56400\sqrt{n_\mathrm{e}[\mathrm{cm}^{-3}]} \approx 1.8 \times 10^{18}\ 1/s \\ \lambda_\mathrm{p} &\approx 105.6/\sqrt{n_\mathrm{e}[10^{17}\mathrm{cm}^{-3}]}[\mu\mathrm{m}] = 105.6\ \mu\mathrm{m}. \end{aligned}$$

It is worth noting that the Debye Shielding assumes a thermalized plasma and is not the right idea of a plasma reaction to a rapid change in charge on a femtosecond timescale. The more appropriate figure of merit in that case is the depth an electromagnetic wave with frequency ω can permeate the plasma fluid given by the skin depth

$$k_\mathrm{p}^{-1} = \frac{c}{\sqrt{\omega_\mathrm{p}^2 - \omega^2}}. \tag{1.12}$$

1.2.1 time scales

scattering can be talked about

1.2.2 plasma definition

There are different types of plasmas, but we are only handling with thin, cold weakly coupled plasmas

1.2.3 electromagnetic waves in plasmas

dispersion relation needs to be talked about. Especially the dispersion relation of lasers during ionization should get some insight here. One has to look into ionization defocussing.

Wavebreaking limit:

$$E_{\mathrm{WB}} = cm_{\mathrm{e}}\omega_{\mathrm{P}}/q_{\mathrm{e}} \simeq 96\sqrt{n_{\mathrm{e}}(\mathrm{cm}^{-3})} \tag{1.13}$$

1.2.4 laser ionisation description

(see diss by Ihar Shchatsinin FU Berlin)

1.2.5 Keldysh Parameter

With E_{bind} being the binding energy and $U_p = \frac{q^2 I}{2m_e\epsilon_0 c\omega^2}$ being the ponderomotive energy

$$\gamma = \sqrt{\frac{E_{bind}}{2U_p}} \tag{1.14}$$

$\gamma > 1$ -¿ Multiphoton Ionisation
$\gamma < 1$ tunnel ionisation or BSI

1.2.6 ADK theory

Tunnel ionization is great

1.2.7 waves in plasmas

So far everything still flows niocely with working along Chen and Mulser. However now the turn needs to be taken. The reason is wavebreaking

1.2.8 wavebreaking

Wavebreaking gives us the the ideal way to go from plasma description to blowout description.

1.3 PWFA theory

1.3.1 History of PWFA

A short historic overview is given. Maybe mention landau damping? Then of course, Tajima,Dawson. Also MTV and Rosenzweig should be mentioned.

1.4 The linear regime

Herleitung by esarey [2]

$$E_\xi = 4\pi \int_0^\xi \rho\xi' \cos(k\mathrm{P}(\xi - \xi'))d\xi \tag{1.15}$$

The transformer ratio $R_{\text{trans}} = \frac{E^+_{\text{max}}}{E^-_{\text{max}}}$ in PWFA is defined as the ratio of the maximum accelerating electric field behind the driving bunch, E^+_{max}, to the maximum decelerating E^-_{max} electric field acting upon drive beam electrons. Experimentally the transformer ratio is comparably easy access-able if one assumes the acceleration length for the witness beam and deceleration length for the drive beam to be equal and that the witness beam is in accelerated at the peak accelerating field. Then it can be observed in the electron energy spectrum as the maximum energy gain of the witness beam divided by the maximum energy loss of the drive beam. In that sense the transformer ratio is a measure of efficiency with which the drive electron beam can transfer energy to the witness electron beam. In the linear regime for a Gaussian drive beam In [3] it is calculated and simulated that the transformer in the linear regime, which is otherwise limited to $R_{\text{trans}} \leq 2$ for a symmetric drive beam current profile [4], can reach up to $R_{\text{trans}} \approx 6.12$ by applying a triangular shaped drive beam current.

1.5 The blowout regime

1.6 Descriptions for the blowout regime

Lotov, Suk, breakdown of fluid theory Q-tilde and resonant wake excitation.

1.7 Accelerator physics

In the previous chapters we examined the physics of the beam driven plasma wake excitation. The ultimate goal as presented in this work is to advantageously make use of the fields in order to inject and accelerate a high quality secondary electron beam, which is conventionally called the witness beam. If there are no substantial advantages between using the witness over the drive beam for a given application, it might not be worth the effort beyond a scholastic interest. In this section we will explain the basic electron beam behavior in an accelerator and from that determine the most important parameters.

1.7.1 Single particle movement

We start with the

$$\vec{F} = \frac{d\vec{p}}{dt} = q(\vec{E} + \frac{\vec{v}}{c} \times \vec{B}) \tag{1.16}$$

Similar to the assumptions made in par-axial optics the electron can be expected to follow a straight trajectory in the absence of any deflecting or accelerating force and any small change in that trajectory can be expressed in a number of linear changes. As in par-axial optics this gives the possibility to describe the electron beam trajectory with linear transformations, represented by a matrix formalism. This idea can be extrapolated to the entire phase-space information of an electron, so that equation

$$\Phi_\mathrm{f} = \hat{R}\Phi_\mathrm{i}$$
$$\begin{pmatrix} x_\mathrm{f} \\ x'_\mathrm{f} \\ y_\mathrm{f} \\ y'_\mathrm{f} \\ z_\mathrm{f} \\ \delta_\mathrm{f} \end{pmatrix} = \begin{pmatrix} R_{11} & R_{12} & R_{13} & R_{14} & R_{15} & R_{16} \\ R_{21} & R_{22} & R_{23} & R_{24} & R_{25} & R_{26} \\ R_{31} & R_{32} & R_{33} & R_{34} & R_{35} & R_{36} \\ R_{41} & R_{42} & R_{43} & R_{44} & R_{45} & R_{46} \\ R_{51} & R_{52} & R_{53} & R_{54} & R_{55} & R_{56} \\ R_{61} & R_{62} & R_{63} & R_{64} & R_{65} & R_{66} \end{pmatrix} \begin{pmatrix} x_\mathrm{i} \\ x'_\mathrm{i} \\ y_\mathrm{i} \\ y'_\mathrm{i} \\ z_\mathrm{i} \\ \delta_\mathrm{i} \end{pmatrix} \tag{1.17}$$

describes a complete linear transformation of an electron's phase space vector as a conservative force acts upon it, with the spatial components x, y, z, the transverse momenta $x' = \frac{p_\mathrm{x}}{p_\mathrm{z}}, y' = \frac{p_\mathrm{y}}{p_\mathrm{z}}$ and the deviation $\delta = \frac{\delta p_\mathrm{z}}{p_\mathrm{z}}$ from the design momentum p_z The matrix $\mathbf{R}_{\mathrm{m,n}} = \frac{\delta\Phi_\mathrm{n}}{\delta\Phi_\mathrm{n}}$ is the Jacobian of this transformation and as that it requires $\det(\hat{R}) = 1$.

Wiedemann: [5]

Jamies book: [6]

1.7.2 Liouville Theorem

When now considering an entire bunch of electrons it comes in handy to describe it as a smooth phase space distribution $f(\vec{r}, \vec{p})$, which is conventionally normalized so that

$$\int_{-\infty}^{\infty} f(\vec{r}, \vec{p}) d\vec{r} d\vec{p} = 1. \tag{1.18}$$

The Liouville Theorem states that if only conservative forces are applied to the bunch the total phase volume occupied by the distribution stays constant. This is mathematically equivalent to any transformation that maintains condition (1.18), which can be expressed by Jacobian transformations of the kind described by equation (1.17). Of course $\hat{R}$ does not need to act upon the entire 6D-Phase space. In fact it is common to reduce the analysis and describe only changes in the transverse phase space, the so called *trace space*, as the planes are mathematically independent and often beam-optics that only influence one plane such as quadropoles or dipoles are applied.

In order to obtain a measure of the actual phase space volume the statistical moments of the distribution can be determined by evaluating the integral

$$< x^n >= \int_{-\infty}^{\infty} f(\vec{r}, \vec{p}) x^n dx. \tag{1.19}$$

1.7.3 Courant-Snyder coefficients, brightness and emittance

Courant and Snyder with their summary paper [7] have set the standard for defining the phase space volume in the trace space with an ellipse equation for its boundary

$$\gamma < x^2 > +2\alpha < x >< x' > +\beta < x'^2 >= \epsilon. \tag{1.20}$$

$$\alpha = \frac{< x^2 >}{\epsilon}, \gamma = \frac{< x'^2 >}{\epsilon}, \alpha = \frac{< xx' >}{\epsilon} \tag{1.21}$$

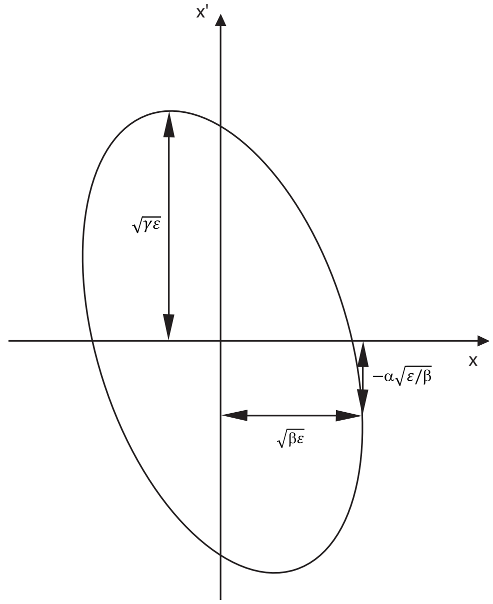

are the so called *Courant Snyder parameters* and ϵ is the trace space emittance. As $f(\vec{r},\vec{p})$ is considered to be smooth function, it might as well consist of a distribution that only approaches 0 so that it is difficult to draw a absolute volume edge as depicted in figure (**??**). Because of this and for the sake of simplicity in comparing the value with experimental data, it is useful to work with the rms values. So the *rms trace space emittance* according to [8] is

$$\epsilon_{\mathrm{tr,rms}} = \sqrt{< x^2 >< x'^2 > - < xx' >^2}. \tag{1.22}$$

This can additionally be normalized to the *normalized rms trace space emittance* into the form

$$\epsilon_{\mathrm{n,tr,rms}} = \frac{p_{\mathrm{z}}}{m_{\mathrm{e}}c}\sqrt{< x^2 >< x'^2 > - < xx' >^2} \tag{1.23}$$

so that its value stays current during acceleration.

The emittance is an important value, as it is invariant under conservative transformations and therefore an important figure of merit for electron beam quality in general. Definition (1.23) will mostly be applied in the context of this work.

Floettmann

1.7.4 Panowsky-Wenzel Theorem

original paper: [9]

$$W_r = \partial_r W_z \tag{1.24}$$

This theorem is so important, it clearly needs a subsection. But where ?

1.8 Electron Trapping in plasma accelerators

In order to derive an expression for the trapping condition of a single electron in PWFA, one has to start with the equation of motion for such a single electron.

$$\vec{F} = \frac{d\vec{p}}{dt} = q(\vec{E} + \frac{\vec{v}}{c} \times \vec{B}) \tag{1.25}$$

with the electron charge q electric field $\vec{E}$ and magnetic field $\vec{B}$

This leads to the single particle electron hamiltonian $H = \gamma mc^2 + \Phi$ with the temporal derivative.

$$\begin{aligned}
\frac{dH}{dt} &= \frac{d}{dt}(\gamma m_e c^2) + \frac{d}{dt}(q\Phi) && (1.26)\\
&= \vec{v}\frac{d\vec{p}}{dt} + \frac{d}{dt}(q\Phi) && (1.27)\\
&= q\vec{v}(-\nabla\Phi - \frac{\partial\vec{A}}{\partial t}) + \frac{\vec{v}\times\vec{B}}{c} + \frac{d}{dt}(q\Phi) && (1.28)\\
&= q(\frac{d}{dt}\Phi - \vec{v}\vec{\nabla}\Phi - \vec{v}\frac{\partial\vec{A}}{\partial t}) && (1.29)\\
&= q(\frac{\partial\Phi}{\partial t} - \vec{v}\frac{\partial\vec{A}}{\partial t}) && (1.30)
\end{aligned}$$

If one assumes now, that the wake fields are constant during the trapping process, then

$$(\frac{\partial}{\partial t} + v_\phi\frac{\partial}{\partial z})f = f(z - v_\phi t) \tag{1.31}$$

$$(\frac{\partial}{\partial t} + v_\phi\frac{\partial}{\partial z})f = 0 \ \forall \ f(\vec{r}, z - v_\phi t) \tag{1.32}$$

which is especially true for the hamiltonian.

$$\begin{aligned}
\frac{d}{dt}H &= q(\frac{\partial\Phi}{\partial t} - \vec{v}\frac{\partial\vec{A}}{\partial t})\\
&= -qv_\phi(\frac{\partial\Phi}{\partial z} - \vec{v}\frac{\partial\vec{A}}{\partial z})
\end{aligned}$$

Since $H - v_\phi P_z = \text{const.}$

$$\begin{aligned}
H - v_\phi P_z &= \text{const.} && (1.33)\\
\gamma mc^2 + \Psi - v_\phi p_z - v_\phi q A_z &= \text{const.} && (1.34)\\
\gamma + \frac{q\Phi}{mc^2} - v_\phi\frac{p_z}{mc^2} &= \text{const.} && (1.35)\\
\gamma - v_\phi\frac{p_z}{mc^2} - \underbrace{\frac{q}{mc^2}(\Phi - v_\phi A_z)}_{\bar{\Psi}} &= \text{const.} && (1.36)
\end{aligned}$$

$\bar{\Psi}$ is the trapping potential, that determines the potential difference for an electron in a potential that moves with a phase velocity v_ϕ with respect to the laboratory frame. It is valid for small as for relativistic velocities. With the trapping potential one can calculate if an electron inside the plasma wake will be accelerated or not i.e. if electrons will be able to catch up with the wake's velocity during the propagation of the wake or if it will slip out of the potential. From the prior calculations a general formula can be determined, that compares

$$\Delta\bar{\Psi} = \bar{\Psi}_{\mathrm{i}} - \bar{\Psi}_{\mathrm{f}} = \gamma_{\mathrm{f}} - \gamma_{\mathrm{i}} - \gamma_f \frac{v_\phi v_{\mathrm{f}}}{c^2} + \gamma_{\mathrm{i}} \frac{v_\phi v_{\mathrm{i}}}{c^2} \tag{1.37}$$

In order to honor the name "trapping potential" i.e. to apply this derivation to make predictions of the electron trapping behavior in the plasma wake, it is necessary to define a trapping condition. An obvious and conventional choice is that an electron should catch up with the wake's velocity so that $v_{\mathrm{f}} = v_\phi$. Equation 1.37 consequently simplifies to

$$\Delta\bar{\Psi} = \gamma_\phi - \gamma_{\mathrm{i}} - \gamma_\phi \frac{v_\phi^2}{c^2} + \gamma_{\mathrm{i}} \frac{v_\phi v_{\mathrm{i}}}{c^2} \tag{1.38}$$

Equation 1.38 can be further separated into different physical cases:

luminal wakefield, electron injected at rest

In this case the plasma wake travels with a phase velocity near the speed of light, which is the case for beam-driven scenarios with high γ driver beams ($v_\phi \approx c$), and electrons starting inside the wake initially at rest ($v_{\mathrm{i}} \approx 0$). Here Equation 1.38 simplifies to

$$\Delta\bar{\Psi} = -1 \tag{1.39}$$

Examples of this case are the underdense photocathode, or Trojan Horse injection [10], or wakefield induced ionization injection [11].

luminal wakefield, electron injected with v $\neq 0$

$$\Delta\bar{\Phi} = -\gamma_{\mathrm{i}}(1 - \frac{v_{\mathrm{i}} v_\phi}{c^2}) \approx -\gamma_{\mathrm{i}}(1 - \frac{v_{\mathrm{i}}}{c}) \tag{1.40}$$

subluminal wakefield, electron injected at rest

$$\Delta\bar{\Psi} = \gamma_\phi(1 - \frac{v_\phi^2}{c^2}) - 1 = \gamma_\phi^{-1} - 1 \tag{1.41}$$

This formula can for example be applied to ionization injection in LWFA [12] or beam-driven ionization injection schemes in which the wake's phase velocity is retarded such as the Downramp-assisted Trojan Horse (DTH) [13], which this work has as special focus on. In latter case mathematically strictly speaking $\frac{dH}{dt} \neq 0$, but for small changes $\frac{dH}{dt} \approx 0$ during the injection process of the electrons, equation 1.41 can still be applied.

superluminal wakefield

There are physical situations imaginable in which the wake or at least part of the wake move with a phase velocity faster than the speed of light. This is the case for example when a beam driven wake traverses an electron density upramp. From the previous deductions it seems obvious, that trapping electrons in such a superluminal wakefield is not possible, as γ_ϕ^{-1} becomes complex for $v_\phi > c$.

However, if the superluminosity is only transient as with a short density upramp, the phase velocity will return to c right after the transition. In this case trpping can be possible, but the mathematic tool presented in this section is insufficient to describe the trapping and the phase velocity after the transition is setting the demand on the potential.

1.8.1 Trapping position and bunch compression

Assuming that the longitudinal wake field $\frac{\partial E_z}{\partial r} = 0$ for a sufficiently wide radius the trapping behaviour can be seen in 1D only. In the blowout regime the acceleration gradient is to a good degree linear in ξ with

$$E_\mathrm{z}(\xi) = \frac{1}{2} k_\mathrm{p} \xi. \tag{1.42}$$

One should keep in mind that the origin of the coordinate system has been shifted so that $\xi = 0$ is at the zero-crossing of the electric field. Integrating erquation 1.42 gives the linear potential

$$U_\mathrm{z}(\xi) = k_\mathrm{p} \xi^2. \tag{1.43}$$

Now equation 1.43 is inserted in equation 1.39 and rearranged in order to find for an electron released at an inital position ξ_i its trapping position ξ by deriving

$$U_\mathrm{z}(\xi_\mathrm{i}) - U_\mathrm{z}(\xi_\mathrm{f}) = -\frac{m_\mathrm{e} c^2}{q_\mathrm{e}} \tag{1.44}$$

$$k_\mathrm{p}(\xi_\mathrm{i}^2 - \xi_\mathrm{f}^2) = -\frac{m_\mathrm{e} c^2}{q_\mathrm{e}} \tag{1.45}$$

$$\xi_\mathrm{trap} = \sqrt{\xi_\mathrm{i}^2 - \frac{m_\mathrm{e} c^2}{q_\mathrm{e} k_\mathrm{p}}}. \tag{1.46}$$

Equation 1.46 is now the relation between release and trapping position of an electron in the co-moving frame for an accelerating field approximated to be linear.

This finding can also be used to calculate the compression of a released electron beam during the trapping. For that we start with a 1D spatial Gaussian distribution with rms length σ_ξ. We will later see that this assumption in fact resembles very well the distribution of interest.

$$f(\xi) = \frac{\sigma_\xi}{\sqrt{2\pi}} e^{-\frac{\xi^2}{2\sigma_\xi^2}}. \tag{1.47}$$

The distribution should be normalized to

$$\int_{-\infty}^{\infty} f(\xi) d\xi \overset{!}{=} 1. \tag{1.48}$$

Equation 1.47 is now

Anderson,Serafini: [14, 15]

emittance preservation

why don't you ... look at space charge effect to estimate required gamma/acceleration and focusing forces for emittance preservation ? Try looking at Pak's thesis and this emittance paper that claims one needs a fast acceleration, but knows nothing about Trojan Horse yet.

1.9 Injection methods in PWFA

1.9.1 Downramp injection

1.9.2 Plasma Torch

1.9.3 Transverse injection ?

1.9.4 ionization injection

It could be discussed here how a witness generation might be different for the wake electric fields. For example, there is no movement of the release position in xi. But the release won't happen in the potential minimum.

1.10 Influence of the ionization behaviour

Here it is to be described how for TH the co-moving frame is advantagous. dependence of ionization front to create witness beams. Image of Ionization front.

1.10.1 Trojan Horse injection

1.10.2 Downramp assisted Trojan Horse

1.11 numerical modeling of Trojan Horse injection

1.11.1 Movement of ionization front

1.11.2 emittance growth from space charge

1.11.3 Laser parameter variations

2. EXPERIMENT

In 2014 the experimental campaign for demonstrating the proof-of-concept of Trojan Horse injection (see 1.10.1) started at the Facility for Advanced Accelerator Experimental Tests (FACET) at the SLAC national laboratory as the experiment E210. It was a collaborative effort with researchers from the University of Hamburg, University of California Los Angeles (UCLA), University of Strathclyde Glasgow and Radiabeam technology with a devoted support from the SLAC personnel. The FACET experiments had to be designed to be non-excluding, which led to a fruitful joint learning process between several groups. It is fair to say that E210 was one of the most complex and accuracy-wise most demanding experiments conducted so far at FACET. Several steps were required in improving the overall setup, until the experiment was eventually successful. The most crucial obstacles to overcome were timing and alignment between two laser arms and the electron beam. The timing requirements between the electron beam and the pre-ionization laser are rather soft as long as the pre-ionization occurs before the arrival of the electron beam an with a timing difference less then the recombination time (ns-s range). However, proper control over relative time-of-arrival between the injection laser and the electron beam required - in principal - control over timing on the order of 10 fs. With an expected timing jitter in the range of 200 fs the best solution here was to accurately measure the relative TOA with an electro-optical sampling (described in2.2) to determine the injection properties from the data, rather than hope for live-control. For finding the synchronization (t_0) as well as fine-alignment between electron beam and injection laser, a newly observed effect on the plasma glow described in 2.4 was measured and applied.

2.1 The FACET experimental setup

2.1.1 LINAC

2.1.2 The FACET laser system

Good description of FACET laser system in [16]

2.1.3 Imaging spectrometer

2.1.4 Laser energy calibration

The FACET laser system ... The energy that can be used on target of the OAP is controlled at two points in the laser-beamline. At each point a cube-polarizer is surrounded by two $\lambda/2$-waveplates, where the upstream one is motorized. The main energy waveplate is located in the laser-room and the probe-energy waveplate is located in the tunnel area shortly after the split between main laser path and probe laser path at the main sampler, which means that the probe laser energy is determined by both waveplate settings while the main laser energy is set by the main laser energy waveplate only. From the power-meter in the laser-room, that measures shot-by-shot laser pulse energy, all the way down to the tunnel a variety of optical components are used until the laser is finally focused onto the The typical shot-to-shot laser energy jitter is ≈ 5% FWHM.

Manta Cameras: [17]

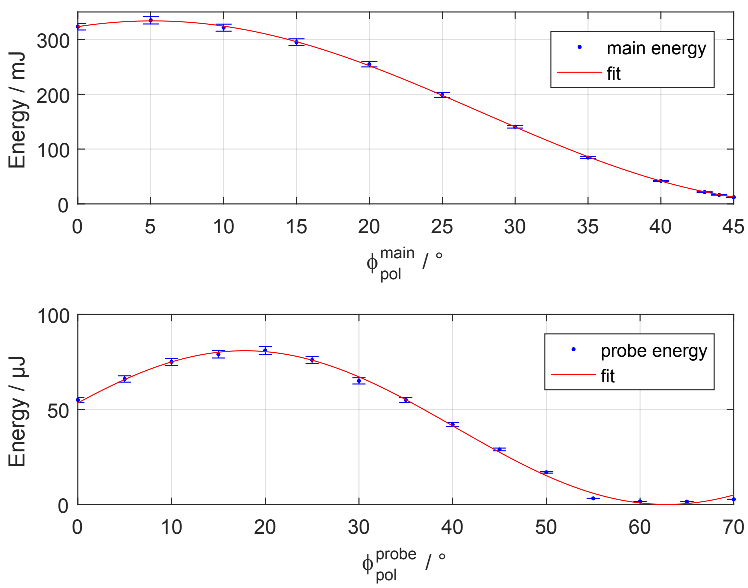

Fig. 2.1: Laser energy calibration for main energy waveplate (upper plot) and probe energy waveplate (lower plot)

All measured losses in optical components combined with the fitted functions for the waveplate energies (see figure 2.1) combined give the on target energy applicable by axilens and OAP respecively.

$$\begin{aligned} W_{\text{Laser}}^{\text{OAP}} = W_{\text{Laser}}^{\text{Laserroom}} &\times 1.25 \times 10^{-2} \\ &\times \left(0.994 \cos^2((\phi_{pol}^{main} - 5.11°)) + 1.16 \times 10^{-3}\right) \\ &\times \left(0.998 \cos^2((\phi_{\text{pol}}^{\text{probe}} - 17.8°)) + 1.62 \times 10^{-3}\right) \end{aligned}$$

$$W_{\text{Laser}}^{\text{Axilens}} = W_{\text{Laser}}^{\text{Laserroom}} \times 0.253 \tag{2.1}$$

$$\times \left(0.994 \cos^2((\phi_{\text{pol}}^{\text{main}} + 66.9°)) + 1.16 \times 10^{-3}\right) \tag{2.2}$$

$$\tag{2.3}$$

This means that for a typical laser energy output of 500 mJ a maximum energy of 6.2 mJ on OAP target and 125.9 mJ on axilens could be used.

2.2 Electro Optical Sampling (EOS)

Electro-optical sampling is a method that allows for determining time-differences in Time-of-arrival between a laser-pulse and a Thz-source, as e.g. an ultra relativistic electron-beam, by exploiting the properties of optically anisotropic crystals and has been shown to be able to measure sub-picosecond electron bunches [18].

Electromagnetic waves, propagating through anisotropic crystals perceive a difference in dielectric permitivity ϵ_{r}, depending on entrance angle and polarization of the wave, which is why in a more general way the dielectric properties need to be addresses with the dielectric permitivity tensor $\hat{\epsilon}$. This is equivalent to a polarization-depending index of refraction, a property known as birefringence, which leads to a polarization-dependent phase velocity of light inside the crystal. A laser at the correct incident angle with respect to an anisotropic crystal will therefore notice a phase shift between different planes of polarization which leads to an overall change in the laser polarization, depending on the phase shift strength and the crystal size. Electro-optical crystals change the orientation of the dielectric permitivity tensor when an external electric field $\vec{E}_{\mathrm{ext.}}$ is applied. The strength of this effect can be illustrated by taylor-expanding the impermeability tensor

$$\hat{\eta} = \hat{\epsilon}^{-1} \tag{2.4}$$

for small external electric fields $\vec{E}_{\mathrm{ext.}}$ to

$$\eta_{ij} = \eta_{ij}(0) + r_{ijk}E_k + s_{ijkl}E_kE_l + \ldots \, . \tag{2.5}$$

The linear dependency on the electric field strength is called Kerr-effect with r_{ijk} being the Kerr-coefficient. The Pockels effect with the Pockels coefficient s_{ijkl} describes quadratic dependency. In the context of this work and the described experiment only two elctro-optical crystals were used, GaP and ZnTe. As both of them are packed in a zincblende geometry, which does not obtain an inversion center, the electro-optic effect is dominated by the Kerr-effect.

EOS setup

In order to measure the relative time-of-arrival between electron bunch and laser pulse an Electro optical sampling (EOS) was set up as a non-destructive shot-by-shot diagnostic.

In this experiment the crystal is located in close proximity (few mm distance) to the electron beam axis. Due to the high $\gamma_{\mathrm{b}} \approx 42000$, the beam electric field is strongly lorenz-contracted and can be assumed to temporally only extend for the length of the electron beam. Consequently the electric field applied to the crystal and with that the induced birefringence are only active while the electron beam passes by the crystal. Figure 2.2 depicts the setup. A linear polarized laser pulse (red), a pickup of the probe beam, traverses the crystal with an angle of $45°$ with respect to the electron beam axis (green). The laser beam is collimated with a transverse diameter of $1cm$ and completely illuminates the crystal. For a better signal-to-noise ratio, an additional polarizing filter was installed prior to the picnic basket chamber. After the chamber follows a cross-polarized filter, which can remotely be rotated for alignment purposes.

During the measurement only the polarization of that transverse part of the laser which propagates through the crystal at the very moment in which the electron beam' electric field induces the birefringence will be rotated and not be filtered by the polarizing filter further downstream the laser beam path. As a result the signal has the form of a line as seen in figure 2.3 with a horizontal position linearly corresponding to the relative TOA.

Fig. 2.2: Setup of upstream electro-optical sampling inside the picnic basket chamber. Electron beam (green) and EOS laser (red) co-propagate in a small angle

The crystal plate is oriented perpendicular to the electron beam axis to minimize temporal overlap and the laser has an ≈ 40 angle with the electron beam which enables a correlation between signal position i.e. the part of the laser with rotated polarization and relative timing.

The entire ladder supports a YAG crystal to find the electron beam axis, a 500 m thick ZnTe for broad timing scans and GaP with 100 m thickness for fine resolution. A detailed description of the physics involved in the application of electro-optical crystals as TOA and bunch length diagnostic can be found in [19].

EOS calibration

For the calibration of the EOS timing, scans were performed in which the arrival time of the laser was altered by changing its path length.

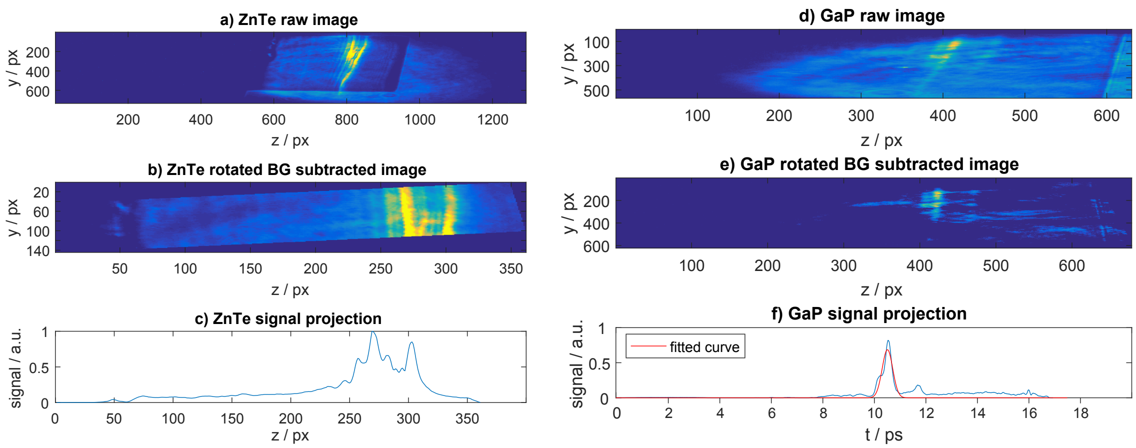

Fig. 2.3: EOS signal

2.3 Ionization test

2.3.1 window B-Integral

2.4 Plasma glow diagnostic

One huge advantage of the hydrogen FACET setup compared to the oven setup is that now several view ports allow for observing the interaction or **??**.

The plasma glow diagnostic as a very simple tool, that turned out to be extremely helpful in controlling the alignment and synchronization of the experimental setup. The main idea is to have a camera integrate over the recombination light. It was observed that this

Figure 2.5 shows the plasma glow accumulated intensity at the wavelength 656±10 nm , sorted by relative time-of-arrival between electron beam as measured by the EOS. The transition between a situation where the injection laser arrives earlier than the electron beam and vice versa is around 1 ps wide, which sufficiently fulfills the requirements to find a range of synchronization as the total range of the EOS crystal is around 20 ps ???. During the data acquisition the electron beam charge was 3.1 ± 0.17 nC.

Result:

With the

2.5 Result: Plasma Torch injection

2.6 Result: Trojan Horse injection

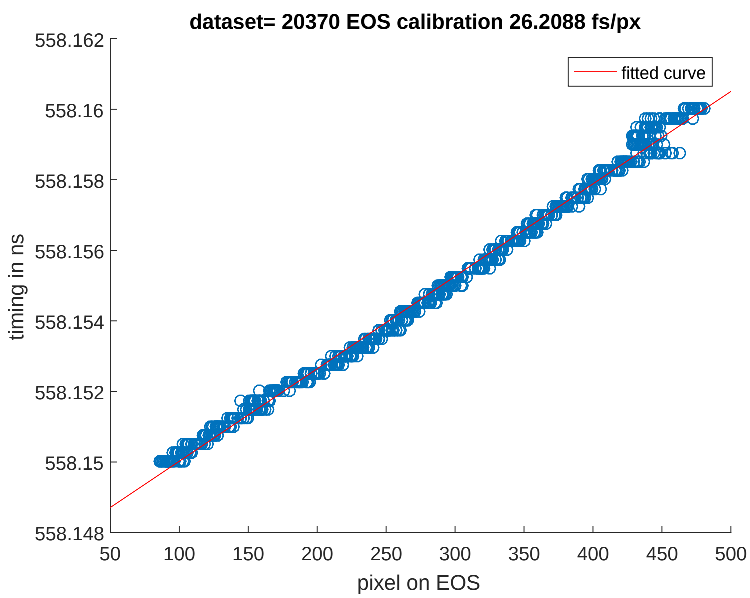

Fig. 2.4: Typical EOS calibration

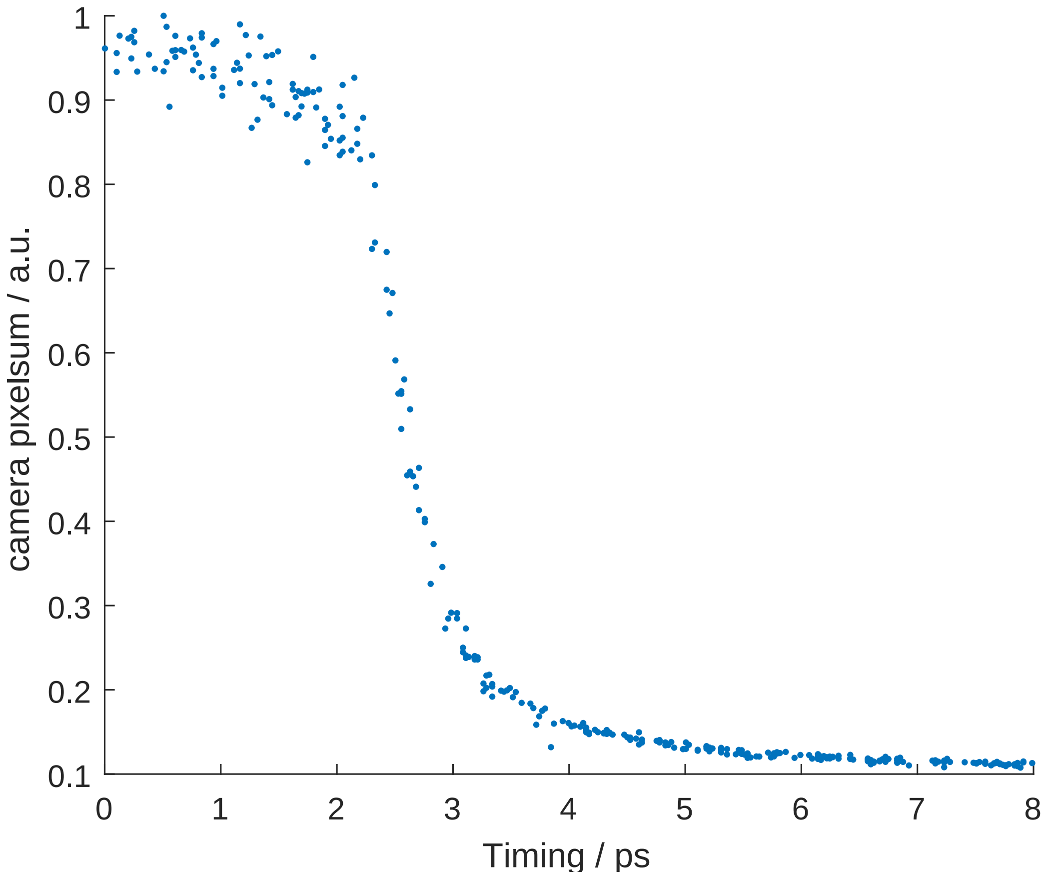

Fig. 2.5: Relative electron beam to injection laser timing scan. The pixel counts measured by the cube 3 vertical camera with a 656±10 nm band-pass filter are sorted by the EOS. evaluation.

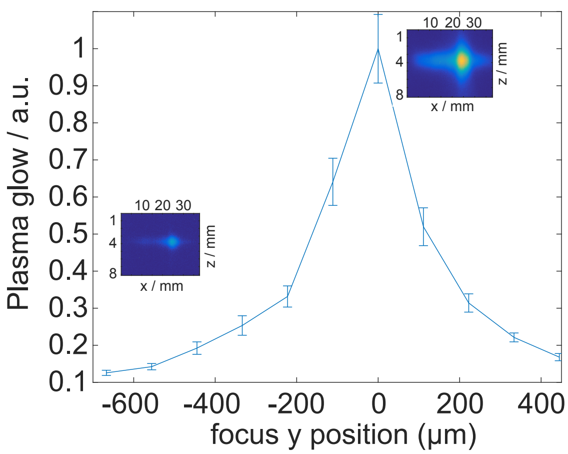

Fig. 2.6: Plasma glow in 7.8 torr H_2 ($n_e = 5 \times 10^{17} \mathrm{cm}^{-3}$) measured by vertical camera in cube 3. The injection laser off-axis parabola roll is scanned. The vertical plasma position is evaluated by the focus diagnostic.

BIBLIOGRAPHY

[1] Francsis F. Chen. *Introduction to Plasma Physics and Controlled Fusion*, volume 1. Plenum Press New York and London, 1974.

[2] E. Esarey, C. B. Schroeder, and W. P. Leemans. Physics of laser-driven plasma-based electron accelerators. *Rev. Mod. Phys.*, 81:1229–1285, Aug 2009.

[3] Pisin Chen, J. J. Su, J. M. Dawson, K. L. F. Bane, and P. B. Wilson. Energy transfer in the plasma wake-field accelerator. *Phys. Rev. Lett.*, 56:1252–1255, Mar 1986.

[4] KL Bane, Perry B Wilson, and T Weiland. Wake fields and wake field acceleration. In *AIP Conf. Proc.*, volume 127, pages 875–928, 1984.

[5] Helmut Wiedemann. *Particle Accelerator Physics*, volume 3. Springer-Verlag, 2007.

[6] J. B. Rosenzweig. *Fundamentals of Beam Physics.* Oxford: Oxford University Press, 2003.

[7] E.D Courant and H.S Snyder. Theory of the alternating-gradient synchrotron. *Annals of Physics*, 3(1):1 – 48, 1958.

[8] Klaus Floettmann. Some basic features of the beam emittance. *Phys. Rev. ST Accel. Beams*, 6:034202, Mar 2003.

[9] W. K. H. Panofsky and W. A. Wenzel. Some considerations concerning the transverse deflection of charged particles in radio-frequency fields. *Review of Scientific Instruments*, 27(11):967–967, 1956.

[10] B. Hidding, G. Pretzler, J. B. Rosenzweig, T. Königstein, D. Schiller, and D. L. Bruhwiler. Ultracold electron bunch generation via plasma photocathode emission and acceleration in a beam-driven plasma blowout. *Phys. Rev. Lett.*, 108:035001, Jan 2012.

[11] A. Martinez de la Ossa, C. Behrens, J. Grebenyuk, T. Mehrling, L. Schaper, and J. Osterhoff. High-quality electron beams from field-induced ionization injection in the strong blow-out regime of beam-driven plasma accelerators. *Nuclear Instruments and Methods in Physics Research Section A: Accelerators, Spectrometers, Detectors and Associated Equipment*, 740:231 – 235, 2014. Proceedings of the first European Advanced Accelerator Concepts Workshop 2013.

[12] A. Pak, K. A. Marsh, S. F. Martins, W. Lu, W. B. Mori, and C. Joshi. Injection and trapping of tunnel-ionized electrons into laser-produced wakes. *Phys. Rev. Lett.*, 104:025003, Jan 2010.

[13] Georg Wittig Henning Groth Yunfeng Xi Aihua Deng James Benjamin Rosenzweig David Leslie Bruhwiler Johnathan Smith Dino Anthony Jaroszynski Zheng-Ming Sheng Grace Gloria Manahan Guoxing Xia Steven Jamison Bernhard Hidding Alexander Knetsch, Oliver Karger.

Downramp-assisted underdense photocathode electron bunch generation in plasma wakefield accelerators. *Physical Review Letters*, 2016.

[14] S. G. Anderson, P. Musumeci, J. B. Rosenzweig, W. J. Brown, R. J. England, M. Ferrario, J. S. Jacob, M. C. Thompson, G. Travish, A. M. Tremaine, and R. Yoder. Velocity bunching of high-brightness electron beams. *Phys. Rev. ST Accel. Beams*, 8:014401, Jan 2005.

[15] L Serafini and M Ferrario. Velocity bunching in photo-injectors. In *AIP conference proceedings*, pages 87–106. IOP INSTITUTE OF PHYSICS PUBLISHING LTD, 2001.

[16] S Z Green, E Adli, C I Clarke, S Corde, S A Edstrom, A S Fisher, J Frederico, J C Frisch, S Gessner, S Gilevich, P Hering, M J Hogan, R K Jobe, M Litos, J E May, D R Walz, V Yakimenko, C E Clayton, C Joshi, K A Marsh, N Vafaei-Najafabadi, and P Muggli. Laser ionized preformed plasma at facet. *Plasma Physics and Controlled Fusion*, 56(8):084011, 2014.

[17] Allied Vision, https://www.alliedvision.com/en/products/cameras/detail/Manta/G-125.html. *Manta G-125 Data sheet*.

[18] X. Yan, A. M. MacLeod, W. A. Gillespie, G. M. H. Knippels, D. Oepts, A. F. G. van der Meer, and W. Seidel. Subpicosecond electro-optic measurement of relativistic electron pulses. *Phys. Rev. Lett.*, 85:3404–3407, Oct 2000.

[19] Bernd Richard Steffen. *Electro-Optic Methods for Longitudinal Bunch Diagnostics at FLASH*. PhD thesis, University of Hamburg, 2007.